Available online at www.sciencedirect.com
ScienceDirect
Journal of the European Ceramic Society 27 (2007) 2753–2757
www.elsevier.com/locate/jeurceramsoc

FDTD analysis of rectangular dielectric resonator antenna

P. Mohanan [a,*], S. Mridula [a], BinuPaul [a], M.N. Suma [a], P.V. Bijumon [b], M.T. Sebastian [b]

[a] *Centre for Research in Electromagnetics and Antennas (CREMA), Department of Electronics, Cochin University of Science and Technology, Kochi 682 022, India*
[b] *Ceramic Technology Division, Regional Research Laboratory, Trivandrum 695 019, India*

Available online 19 December 2006

Abstract

The paper presents basics of electromagnetic theory and dielectric resonator antennas, fundamental concepts of FDTD and some significant results of the FDTD analysis of rectangular dielectric resonator antennas (RDRA).

Keywords: Sintering; Dielectric properties; Perovskites; Insulators

1. Introduction

The electromagnetic force is the most technologically pervasive force in nature. Of the different methods for predicting electromagnetic effects—experiment, analysis and computation—the newest and fastest growing approach is computation. Electromagnetic computational engineering encompasses the modeling, simulation and analysis of the responses of complex systems to various electromagnetic stimuli, allowing for better design or modification of the system. The FDTD method originally proposed by Yee,[1] is an explicit finite difference scheme using central differences on a Cartesian grid staggered in both space and time. The simplicity of the method is noteworthy. Maxwell's equations in a differential form are discretized in space and time in a straightforward manner. The method tracks the time-varying fields throughout a volume of space. The updated new value of a field component (*E*/*H*) at any layer depends upon its value in the previous step and the previous value of the components of the other field at the adjacent spatial points. Thus FDTD results lend themselves well to scientific visualization methods, providing the user with excellent physical insight into the behavior of electromagnetic fields.[2] The geometric flexibility of the method permits the solution of a wide variety of radiation, scattering and coupling problems. Also, desired accuracy can be achieved by selecting suitable discretization parameters and boundary conditions.

Research in compact antenna solution is a priority among antenna researchers due to the increasing quest for compact wireless communication equipment. Dielectric resonator antennas (DRAs) have attracted the attention of investigators ever since their introduction in 1980s.[3,4] They are small sized, devoid of conductor losses, have high radiation efficiency and can be easily excited. Rectangular dielectric resonator antennas are preferred over other geometrical shapes because they are easy to fabricate and offer more degrees of freedom to control the resonant frequency and quality factor.[5]

Some of the significant outcomes of the theoretical and experimental investigations on a Microstrip line excited, high permittivity ($\varepsilon_{rd} = 48$), compact, rectangular dielectric resonator antenna is presented here. The FDTD method is employed to study the reflection characteristics of the DRA at different positions along the feed line. Experimental results are presented to support the theoretical data. Thereafter, far-field distribution of the DRA is predicted and verified by measurements.

2. The antenna configuration

Fig. 1 shows the geometry of the antenna. The antenna comprises of a rectangular dielectric resonator of dimensions ($a \times b \times d$) = 2.25 cm × 1.19 cm × 0.555 cm made of low loss ceramic material $Ca_5Nb_2TiO_{12}$. Of the six possible orientations of the DR upon the feed line, the antenna configuration in the b-a-d orientation of the DR is shown. The DR is prepared using the conventional solid-state ceramic route[6] at a sintering temperature of 1550 °C. The low density of the material (4.05 g/cm^3) ensures lightweight of the antenna configuration.

* Corresponding author. Tel.: +91 484 2576418; fax: +91 484 2575800.
E-mail address: drmohan@cusat.ac.in (P. Mohanan).

0955-2219/$ – see front matter © 2006 Elsevier Ltd. All rights reserved.
doi:10.1016/j.jeurceramsoc.2006.11.053

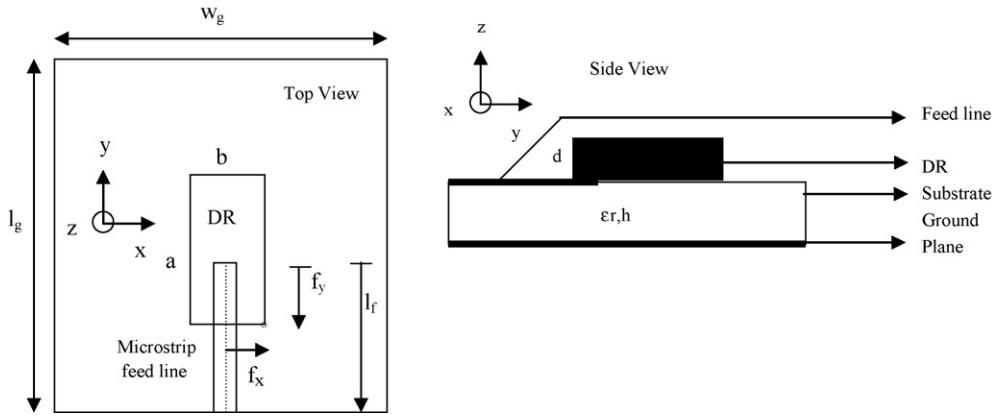

Fig. 1. b-a-d orientation of the DRA upon the feed line. Ground plane dimensions $l_g = 4$ cm, $w_g = 4$ cm, substrate $\varepsilon_r = 4.28$, $h = 1.6$ mm, Feed dimensions $l_f = 2$ cm, and width = 3 mm.

The DR is excited directly by a 50 Ω Microstrip line of width 3 mm, fabricated on a substrate of dielectric constant $\varepsilon_{rd} = 4.28$ and thickness 1.6 mm.

3. The FDTD method of DRA analysis

The FDTD code is written using MATLAB™. To facilitate the implementation of the algorithm in a digital computer, the indices of the field components are renamed, eliminating the 1/2 index notation as suggested by Sheen et al.[7] This allows the value of each field component to be stored in a three-dimensional array, with the array indices corresponding to the spatial indices. A Gaussian voltage source with a series source resistance ($r_s = 50\ \Omega$) is used.[8] The Gaussian pulse of half-width $T = 15$ ps and time delay $t_0 = 3T$ is applied at the source plane. The width of the pulse and the time delay are chosen to suit the frequency bands of interest. The time step used is $\Delta t = 1.155$ ps, satisfying the courant stability condition.

Of the six possible orientations of the rectangular DRA upon the Microstrip feed line, the results for the b-a-d orientation are presented here. The cell size chosen to accommodate more than 20 cells per wavelength within the DR and the substrate is $\Delta x = 0.5$ mm, $\Delta y = 0.5$ mm and $\Delta z = 0.4$ mm. The size of the computational domain is 66 $\Delta x \times 110\ \Delta y \times 33\ \Delta z$. The large amount of data generated during the implementation of FDTD approach on a computer calls for the truncation of the computational domain with artificial boundaries to simulate its extension to infinity, since modelling of an infinite space is numerically impossible. Nevertheless, the computational domain must be large enough to enclose the structure of interest. The perfect electric conductor (PEC) or the electric wall, the perfect magnetic conductor (PMC) or the magnetic wall, the absorbing boundary condition (ABC) and the dielectric interface are the commonly applied boundary conditions.

Mur's first order ABC[9] looks back one step in time and one cell into the space location. A second order condition looks back two steps in time and two cells inward, etc. According to Mur's first order ABC, the tangential electric field components on the outer boundaries will obey the one-dimensional wave equation in the direction normal to the mesh wall. Berenger's PML requires considerable enlargement of the computational volume, but is essentially frequency independent, superior to most ABCs and rather easy to implement. More often, when computer memory and ease of programming is determinative, one uses Mur's ABC, otherwise the choice is PML.

In the present work Mur's First order absorbing boundary conditions are used to terminate the computational domain, the distance from the object to the absorbing boundary being about 10 space steps in each direction. The iterations are performed for 5000 time steps to allow the input Gaussian to converge to zero within the computational domain. The input impedance of the antenna is computed as the ratio of the FFT of the voltage derived from E field values at the observation point over the entire time steps, to the FFT of the current at the same point, derived from the H field values. Reflection coefficient S_{11} (in dB) is then computed. The position of the DR along the feed line is optimized for maximum bandwidth.

The FDTD model is then rerun with a sinusoidal excitation fixed at the resonant frequency of the DRA, as defined by the minimum return loss. Iterations are carried out until the system achieves sinusoidal steady state. An aperture is defined in a layer above the DR surface, as shown in Fig. 2. The far field components E_θ and E_φ are computed using the electric vector potential F derived from the instantaneous tangential E field components over the aperture.[10] The validation of the predicted numerical results with respect to the experimental data is performed in the following section.

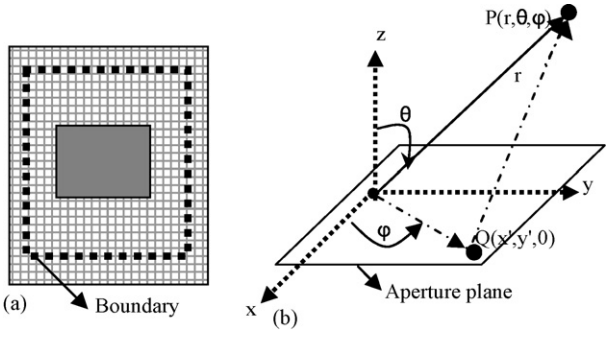

Fig. 2. Pattern computation using FDTD. (a) Aperture boundary in a layer above the DR surface. (b) Spatial point Q in the aperture layer and far field point P.

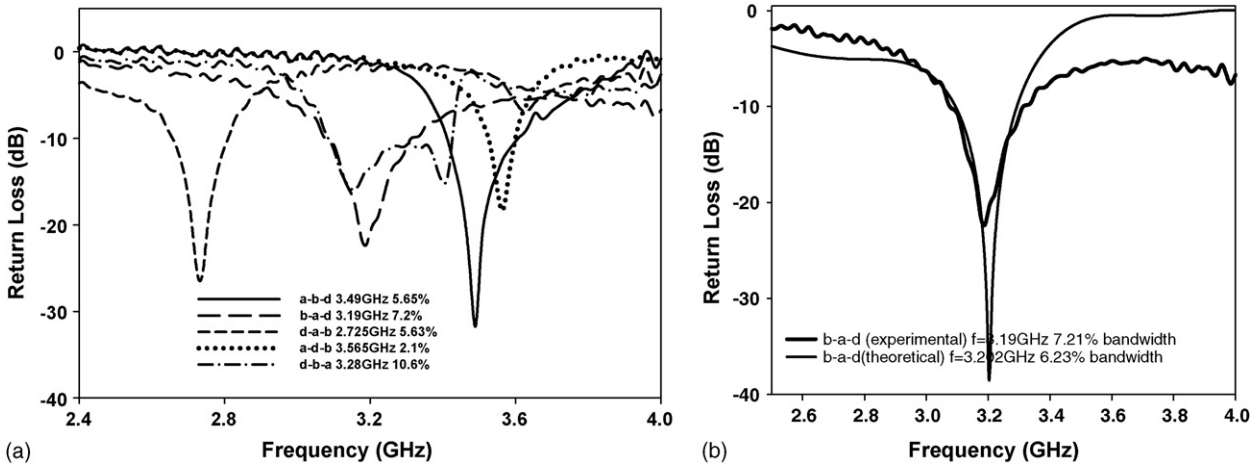

Fig. 3. (a) Reflection characteristics at the optimum band width position of the DR in the various orientations upon the feed line. (b) Reflection characteristics at the optimum band width position of the DR in the b-a-d orientation.

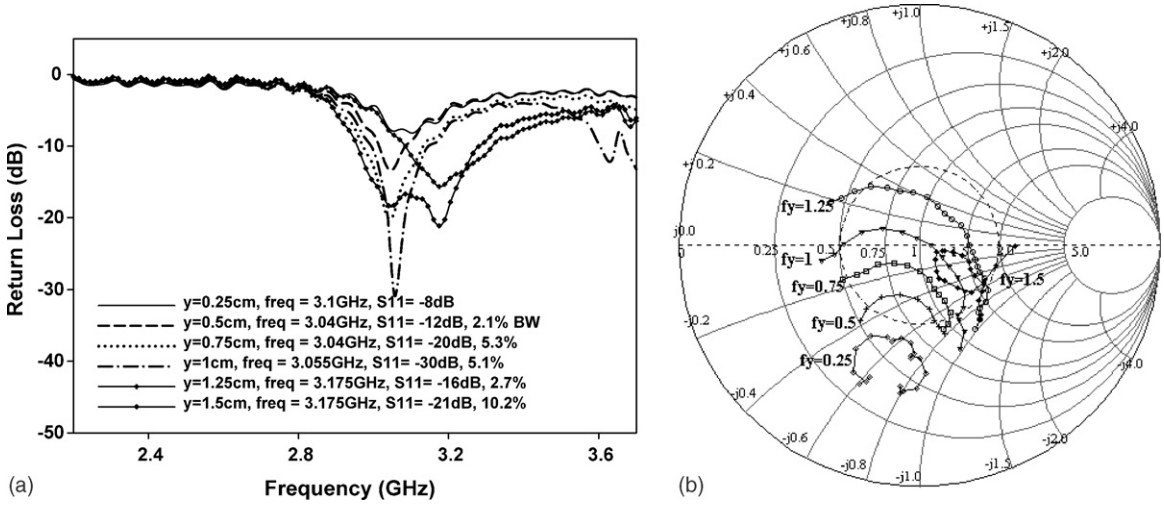

Fig. 4. (a) Return loss of the DRA placed in the b-a-d orientation, and (b) Input impedance loci of the DRA placed in the b-a-d orientation, ($f_x = 0.5$ cm, $f_y = 0.25$, 0.5, 0.75, 1, 1.25, 1.5 cm).

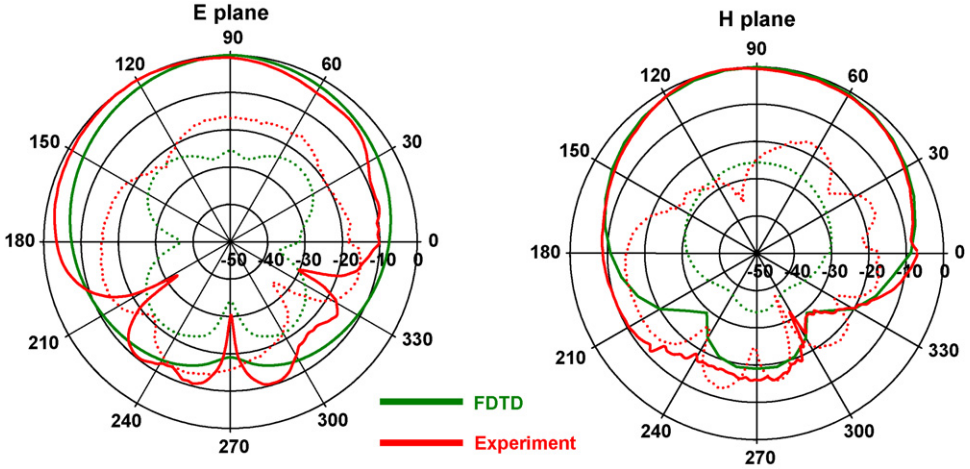

Fig. 5. Radiation pattern of the DRA at the optimum bandwidth position ($f = 3.175$ GHz), (—) co-polar, (. . .) cross-polar, feed line length = 2 cm, ground plane: 4 cm × 4 cm.

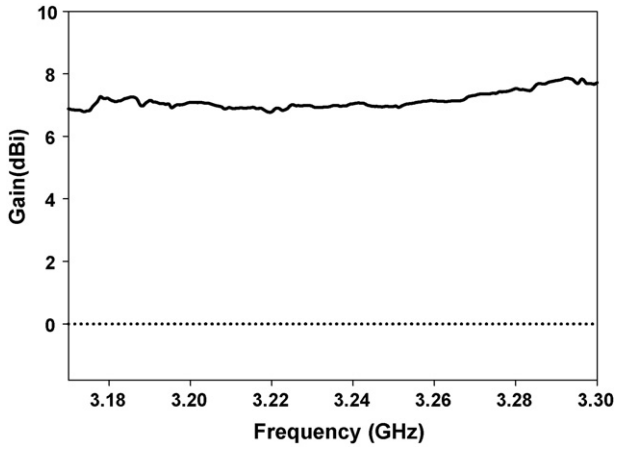

Fig. 6. Gain of the antenna measured in the b-a-d orientation of the DR.

4. Results and discussion

Different resonant frequencies are excited as the DR is moved along the feed line. The return loss for different positions of the DR placed in different orientations along the feed line is measured and optimized for maximum bandwidth. The measurements are done using HP 8510C Network Analyzer. The return loss at the optimum position of the DR (where the numerical results closely relate to the experimental observations) is plotted in Fig. 3(b). The experimentally observed variation in the return loss and input impedance for different positions of the DRA along the feed line is shown in Fig. 4 [$f_x = 0.5$ cm, $f_y = 0.25$, 0.5, 0.75, 1, 1.25, and 1.5 cm]. The figure illustrates the significance of the DR position with respect to the feed line. At (f_x, f_y) = (1.5, 0.5), two closely spaced resonant bands merge to give a wide band characteristic.

The radiation pattern of the DRA is measured for all orientations of the antenna. Fig. 5 shows the radiation pattern of the antenna in the b-a-d orientation, at the optimum bandwidth position. The normalized co-polar far field patterns (E_θ and E_φ) computed for the DRA in the orthogonal E and H planes ($\varphi = 0^\circ$ and 90°) are also shown for comparison. From the simulated studies it is found that at the centre frequency the efficiency of the antenna is 87%. FDTD simulation is repeatedly performed on a Pentium^{TM} IV processor (3.2 GHz), for various grid parameters. It is concluded from the obtained data that the chosen grid parameters is sufficient for obtaining reasonably good agreement with the measured data. The resonant frequency of the antenna can be accurately predicted by the FDTD calculation. However, away from the resonance the discrepancy is more. This can be improved using PML boundary conditions. The proposed antenna configuration also exhibits good gain throughout the band. The measured gain characteristics of the DRA are shown in Fig. 6. The field distribution in the DR placed in the b-a-d orientation is illustrated in Fig. 7. The $TE^z_{11\delta}$ mode is excited at 3.202 GHz with one half cycle variation in the x- and y-directions and less than a half cycle (δ) in the z-direction.

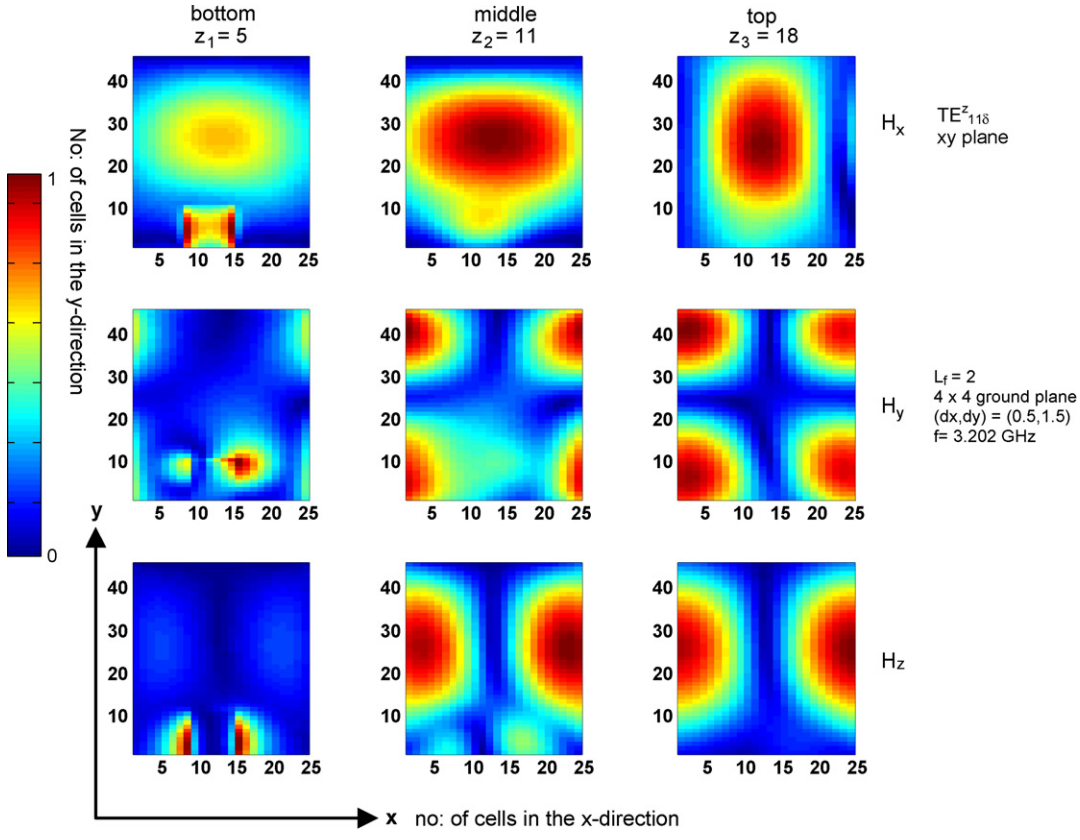

Fig. 7. Resonant modes of the Microstrip fed rectangular dielectric resonator antenna.

5. Conclusion

Investigations on a Microstrip line excited compact rectangular dielectric resonator antenna are performed. The numerical results predicted using FDTD method are compared with the experimental data and good agreement is obtained. The proposed antenna is compact, easily excited and exhibits broad radiation patterns suitable for mobile communication applications.

References

1. Yee, K. S., Numerical solution of initial boundary value problems involving Maxwell's equations in isotropic media. *IEEE Trans. Antennas Propagat.*, 1966, **14**, 302–307.
2. Kunz, K. S., Raymond, J. and Luebbers, R. J., *The Finite Difference Time Domain Method for Electromagnetics*. CRC Press, New York, 1993.
3. Long, S. A., McAllister, M. W. and Shen, L. C., The resonant cylindrical dielectric cavity antenna. *IEEE Trans. Antenn. Propag.*, 1983, **31**, 406–412.
4. Kishk, A. A., Xiao, Z., Glisson, A. W. and Darko, K., Numerical analysis of stacked dielectric resonator antennas excited by a coaxial probe for wideband applications. *IEEE Trans. Antenn. Propag.*, 2003, **51**, 1996–2006.
5. Mongia, R. K. and Ittipiboon, A., Theoretical and experimental investigations on rectangular dielectric resonator antennas. *IEEE Trans. Antenn. Propag.*, 1997, **AP–45**, 1348–1356.
6. Bijumon, P. V., Menon, S. K., Sebastian, M. T. and Mohanan, P., Enhanced bandwidth microstrip patch antennas loaded with high permittivity dielectric resonators. *Microwave Optical Technol. Lett.*, 2002, **35**, 327–330.
7. Sheen, D. M., Ali, S. M., Abouzahra, M. D. and Kong, J. A., Application of the three-dimensional finite- difference time-domain method to the analysis of planar Microstrip circuits. *IEEE Trans. Microw. Theory Tech.*, 1990, **38**, 849–857.
8. Leubbers and Langdon, H. S., A simple feed model that reduces time steps needed for FDTD antenna and Microstrip calculations. *IEEE Trans. Antenn. Propag.*, 1996, **44**, 1000–1005.
9. Mur, G., Absorbing boundary conditions for the finite-difference approximation of the time-domain electromagnetic field equations. *IEEE Trans. Electromagn. Compat.*, 1981, **23**, 377–382.
10. Garg, R., Bhartia, P., Bahl, I. and Ittipiboon, A., *Microstrip Antenna Design Handbook*. Artech House Publishers, 2001.